A 1D Theoretical Analysis of Northerly Low-Level Jets over the Great Plains

JOSHUA G. GEBAUER

School of Meteorology, and Cooperative Institute for Mesoscale Meteorological Studies, University of Oklahoma, Norman, Oklahoma

EVGENI FEDOROVICH

School of Meteorology, University of Oklahoma, Norman, Oklahoma

ALAN SHAPIRO

School of Meteorology, and Center for Analysis and Prediction of Storms, University of Oklahoma, Norman, Oklahoma

(Manuscript received 17 November 2016, in final form 23 July 2017)

ABSTRACT

The forcing of northerly low-level jets over the eastward-sloped terrain of the U.S. Great Plains was studied using a one-dimensional (1D) nonstationary analytical model based on the Boussinesq-approximated equations of motion and thermal energy. For northerly low-level jets, the forcing from diurnal changes in surface heating of the sloped terrain (Holton mechanism) is out of phase with the nocturnal inertial oscillation resulting from the cessation of turbulent mixing at sunset (Blackadar mechanism), which results in weaker northerly nocturnal low-level jets when compared to southerly nocturnal low-levels jets with the same-magnitude background pressure gradient forcing. Because of the Blackadar and Holton mechanisms acting out of phase, nocturnal northerly low-level jets cannot solely explain the northerly low-level jet maximum over the Great Plains found in climatological studies. It is shown that negative buoyancy values over the eastward-sloped terrain enhance the low-level northerly geostrophic wind, which can cause low-level jetlike wind profiles that do not necessarily depend on the diurnal cycle. However, nocturnal northerly low-level jets primarily caused by an inertial oscillation still occur when daytime mixing is strong and buoyancy is small at sunset. These conditions are possible when strong capping inversions are present in the daytime convective boundary layer. The occurrence of both types of northerly low-level jets, those caused by negative buoyancy values over the sloped terrain and those driven by an inertial oscillation, better explains the findings of previous low-level jet climatologies.

1. Introduction

Wind maxima in the lowest levels of the atmosphere have been an intensively studied meteorological phenomenon. Often referred to in the literature as low-level jets (LLJs), these wind maxima can occur as low as 90 m above ground (Banta et al. 2002). Such LLJs can play a role in pollutant mixing and transport (Zunckel et al. 1996; Banta et al. 1998; Darby et al. 2006; Bao et al. 2008; Klein et al. 2014) and can affect wind energy production (Cosack et al. 2007; Storm et al. 2009; Banta et al. 2013).

LLJs are known to occur all over the globe because of a variety of forcing mechanisms. At almost any location, an LLJ can develop because of transient features, such as the ageostrophic circulation of an upper-level jet streak (Uccellini and Johnson 1979; Uccellini 1980) or, more commonly, a nocturnal inertial oscillation (Blackadar 1957). A nocturnal inertial oscillation is a clockwise (in the Northern Hemisphere) turning of the ageostrophic wind vector, which is caused by the release of friction constraint (near cessation of turbulent mixing) during the evening transition. According to Blackadar (1957), LLJs created through inertial oscillations reach their peak intensity when the ageostrophic wind aligns with the geostrophic wind. The wind direction at the time of peak intensity is therefore controlled by the direction of the geostrophic wind. Inertial oscillations can explain most nocturnal LLJs, but they cannot explain why some regions have more frequent

Corresponding author: Joshua G. Gebauer, joshua.gebauer@ou.edu

DOI: 10.1175/JAS-D-16-0333.1

and intense LLJs. In these regions, a local forcing mechanism is the cause of the frequent LLJs. These LLJ corridors are often found in coastal regions or east of a mountain range above sloping terrain (Stensrud 1996). Coastal LLJs, such as the California LLJ (Parish 2000) and the Oman LLJ (Ranjha et al. 2015), are driven by the land–sea temperature contrast. Terrain-induced LLJs, which are the focus of this paper, are the result of thermal effects over the vast sloping terrain west of a mountain range. The most well-known LLJ of this type is the Great Plains LLJ, but other similar LLJs exist, such as the South America LLJ (Vera et al. 2006).

In an attempt to explain the cause of slope-induced LLJs, Holton (1967) suggested that the prevailing occurrence of southerly LLJs over the Great Plains was due to the diurnal heating and cooling of the eastward-sloping terrain in the presence of a southerly free-atmosphere geostrophic wind. This diurnal heating creates a diurnal oscillation in the low-level geostrophic wind, which results in enhanced southerly winds during the early overnight hours. The Holton (1967) explanation, however, was not able to produce LLJs of the correct strength, and the wind maxima occurred too early. Bonner and Paegle (1970) modeled the combined effect of inertial oscillations (Blackadar mechanism) and a diurnally oscillating geostrophic wind (Holton mechanism) and showed that, together, the effects produced stronger southerly LLJs. The two mechanisms are in phase over the eastward-sloped terrain for southerly LLJs. Numerical weather prediction modeling studies agree with this finding but suggest that the inertial oscillation is the dominant mechanism (Zhong et al. 1996). Shapiro and Fedorovich (2009) further examined the role of the sloped terrain on the Great Plains LLJ by adding a thermal energy equation to the original Blackadar consideration and found that LLJs over sloped terrain are actually the result of an inertial-gravity oscillation. Expanding upon this concept, Shapiro et al. (2016), hereafter referred to as SFR16, obtained a one-dimensional (1D) analytical solution for a Great Plains southerly LLJ with parameterized diurnally varying eddy viscosity and surface buoyancy. The obtained analytical solutions were able to reproduce LLJs that were consistent with those observed.

Most of the research on the Great Plains LLJ has focused on the southerly variety since they occur more frequently than LLJs of other directions and also because of the southerly LLJs' association with convective storms (Means 1954; Pitchford and London 1962; Maddox 1983; Trier and Parsons 1993; French and Parker 2010). Climatologies of LLJs over the continental United States (CONUS), however, have shown that a local maximum in northerly LLJs is found in the Great Plains region as well, although their frequency of occurrence does not approach that of southerly LLJs (Bonner 1968; Walters et al. 2008). This secondary maximum in LLJ frequency has not garnered the same research attention as the more common southerly LLJ. Northerly LLJs occur most often during the cold season and are more frequent at higher latitudes (Bonner 1968; Whiteman et al. 1997; Song et al. 2005; Walters et al. 2008). The dependence of frequency on latitude becomes stronger in the summer months, as almost no northerly LLJs occur in the summer at low latitudes (i.e., over south/central Texas), while in the winter months, northerly LLJs occur at all latitudes over the Great Plains (Walters et al. 2008). Overall, northerly LLJs tend to be weaker than southerly LLJs (Song et al. 2005), and there appears to be an association between cold-frontal passages and the development of northerly LLJs (Whiteman et al. 1997). A case study of a post-frontal LLJ was conducted by Ostdiek and Blumen (1997), who determined that deformation frontogenesis and an inertial oscillation produced the LLJ seen in their study. Frontal forcing, however, cannot explain the northerly LLJ maximum since these northerly LLJs could occur with cold fronts in other locations.

There has been disagreement in the LLJ climatologies over the diurnal variation of northerly LLJs. Bonner (1968) and Walters et al. (2008) used twice-daily radiosonde observations to establish their climatologies and found that northerly LLJs were observed more frequently in the 1200 UTC soundings than in the 0000 UTC soundings. Whiteman et al. (1997) used more frequent soundings at the Southern Great Plains Cloud and Radiation Testbed in northern Oklahoma and found that northerly LLJs did not appear to have a significant diurnal variation in wind speed or direction, though the occurrence of northerly LLJs had a weak daytime maximum. It is likely that differences in the data frequencies resulted in the discrepancies between the climatological studies.

The most common explanation for the northerly LLJ maximum over the Great Plains is a higher frequency of synoptic-scale features that produce northerly wind maxima in this region. Walters et al. (2008) mentioned that the northerly LLJ maximum occurs east of the typical wintertime anticyclonic track, and wintertime cyclones also frequent this region. Together, these two features could result in frequent northerly wind maxima. While synoptic-scale features likely do play a role in the occurrence of northerly LLJs, they cannot explain the diurnal variation in the frequency of northerly LLJs found in the Bonner (1968) and Walters et al. (2008) climatologies. In addition, the Walters et al. (2008) climatology clearly shows the northerly LLJ maximum over portions of the Great Plains sloping terrain with the

greatest inclination angles (around 0.15°), which suggests that terrain slope may be a factor. Until now, there has not been a study to specifically explore the roles of the sloping terrain and diurnal planetary boundary layer (PBL) variations in the dynamics of northerly LLJs over the Great Plains.

Since the northerly LLJ maximum is located over the same region as the southerly LLJ maximum, it is reasonable to expect that many of the same processes affecting southerly LLJs also affect northerly LLJs. Therefore, it was decided to use the SFR16 analytical model to study these northerly LLJs. The original SFR16 study restricted the analysis to southerly LLJs, but there is no reason why the model could not be used for studying northerly LLJs.

The layout of the paper is as follows: Section 2 summarizes the SFR16 model and describes its application to reproduce northerly LLJs. In section 3, modeling results are presented and analyzed, and the effects of the model parameter variations on the LLJ development are studied. The discussion of the findings follows in section 4, and a case study is presented to support the discussion. Conclusions follow in section 5.

2. Methods

SFR16 described the Great Plains LLJ dynamics using the following one-dimensional Boussinesq equations of motion and thermal energy written in a slope-following coordinate system (see Fig. 1):

$$\frac{\partial u}{\partial t} = f(v - v_g) - b\sin\alpha + K\frac{\partial^2 u}{\partial z^2}, \tag{1}$$

$$\frac{\partial v}{\partial t} = -fu + K\frac{\partial^2 v}{\partial z^2}, \tag{2}$$

$$0 = -\frac{\partial \Pi}{\partial z} + b\cos\alpha, \quad \text{and} \tag{3}$$

$$\frac{\partial b}{\partial t} = uN^2\sin\alpha - \delta b + K\frac{\partial^2 b}{\partial z^2}. \tag{4}$$

Here, the x axis is directed down the slope, the y axis is directed across the slope, and the z axis is normal to the slope. In Fig. 1, x^* and z^* represent the true horizontal and vertical coordinates, and α is slope angle, assumed to be small in all further considerations (on the order of 0.1°; see SFR16). In (1)–(4), u and v represent the x and y components of the wind, and b is the buoyancy defined as $b \equiv g[\theta - \theta_e(z^*)]/\theta_0$, where θ is potential temperature, $\theta_e(z^*)$ is environmental potential temperature, and θ_0 is a constant reference potential temperature. The normalized pressure perturbation is defined as $\Pi = [p - P(z^*)]/\rho_0$, where p is pressure, $P(z^*)$ is the environmental pressure at a fixed x^* location, and ρ_0 is a constant reference

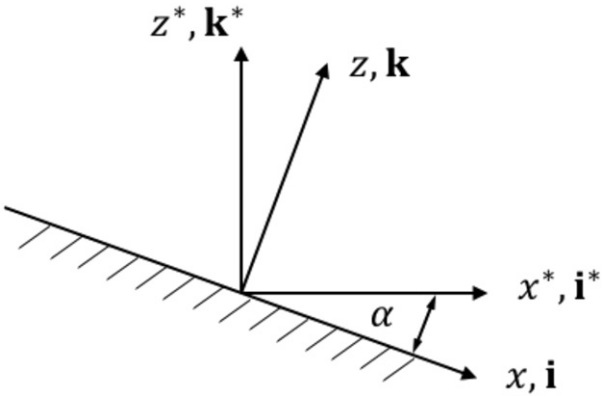

FIG. 1. The slope-following coordinate system used for the analytical solution. Figure is adapted from SFR16 (their Fig. 1).

density. The wind and buoyancy fields are considered to be homogeneous in planes parallel to the slope. The Coriolis parameter, defined as $f \equiv 2\Omega \cdot \mathbf{k}$, where Ω is the angular velocity of Earth's rotation and $\mathbf{k}$ is the unit vector in the z direction, is considered to be constant; the small deviation of this f from the true Coriolis parameter (component of 2Ω in the direction of the unit vector in the z^* direction) is neglected. The free-atmosphere Brunt–Väisälä frequency (also known as buoyancy frequency) $N \equiv \sqrt{(g/\theta_0)\, d\theta_e/dz^*}$, where g is gravity acceleration, is considered constant; δ is a constant radiative damping parameter that is needed to ensure diurnal periodicity of solutions (see SFR16); v_g is a geostrophic wind associated with the perturbation pressure gradient, $v_g = (1/f)(\partial\Pi/\partial x)$. The eddy diffusivity K is taken independent of height and equal for both heat and momentum.

The boundary conditions at the surface are

$$u(0,t) = 0, \quad v(0,t) = 0, \quad \text{and} \quad b(0,t) = b_s(t), \tag{5}$$

where $b_s(t)$ is a diurnally periodic function. Far above the slope, the boundary conditions are

$$\lim_{z\to\infty} u = 0, \quad \lim_{z\to\infty} v = v_{g\infty} = \frac{1}{f}\left(\frac{\partial \Pi}{\partial x}\right)_{\infty}, \quad \text{and} \quad \lim_{z\to\infty} b = 0. \tag{6}$$

These upper boundary conditions ensure that v_g is spatially and temporally constant. Taking $\partial/\partial x$ of (3), reordering the differentiation and dividing by f yields

$$\frac{\partial v_g}{\partial z} = 0, \tag{7}$$

so at most, v_g could be a function of x or t. The upper boundary conditions, however, indicate that v_g cannot

be a function of x or t; v_g must thus equal the free-atmosphere value $v_{g\infty}$. Note that in SFR16, the free-atmosphere geostrophic wind was designated by v_g. In this study, $v_{g\infty}$ is used to designate the free-atmosphere geostrophic wind to make clear that it refers to the geostrophic wind far above the slope.

Eddy viscosity K and surface buoyancy b_s are diurnally periodic and prescribed in the same way as in SFR16. The eddy viscosity is prescribed through the piecewise constant function

$$K(t) = \begin{cases} K_d, & 0 \le t < t_{\text{set}} \\ K_n, & t_{\text{set}} \le t < t_{24} \end{cases}, \tag{8}$$

where K_d and K_n are, respectively, constant daytime and nighttime values of K, $t = 0$ is the time of sunrise, t_{set} is the time of sunset, and t_{24} is 24 h. The surface buoyancy is prescribed through a piecewise linear function:

$$b_s(t) = \begin{cases} b_{\min} + \Delta b\left(\dfrac{t}{t_{\max}}\right), & 0 \le t < t_{\max} \\ b_{\max} - \Delta b\left(\dfrac{t - t_{\max}}{t_{24} - t_{\max}}\right), & t_{\max} \le t < t_{24} \end{cases}, \tag{9}$$

where $b_{\min}$ is the surface buoyancy minimum, $b_{\max}$ is the surface buoyancy maximum, $\Delta b \equiv b_{\max} - b_{\min}$, and $t_{\max}$ is the time of the surface buoyancy maximum.

The analytical solution of the governing (1)–(4) for the prognostic variables u, v, and b with prescribed boundary conditions [(5) and (6)], and K and b_s given by (8) and (9), respectively, is derived in SFR16. The solution is controlled by 11 adjustable external parameters: slope angle α, Coriolis parameter f, free-atmosphere Brunt–Väisälä frequency N, free-atmosphere geostrophic wind $v_{g\infty}$, radiative damping parameter δ, daytime diffusivity K_d, nighttime diffusivity K_n, maximum surface buoyancy $b_{\max}$, minimum surface buoyancy $b_{\min}$, time of maximum surface buoyancy $t_{\max}$, and time of sunset t_{set}. As indicated in SFR16, the analytical solution can represent three different LLJ mechanisms: a pure Blackadar (B) mechanism when $\alpha = 0$ and $K_d > K_n$, a pure Holton (H) mechanism when $K_d = K_n$ and $b_{\max} \neq b_{\min}$, and the combined Blackadar–Holton (BH) mechanism when $\alpha \neq 0$, $K_d > K_n$, and $b_{\max} \neq b_{\min}$. Additionally, although not explicitly discussed by SFR16, the analytical solution can also be applied for the case where the B mechanism acts over heated (or cooled) sloping terrain without diurnal variations in surface buoyancy when $K_d > K_n$ and $b_{\max} = b_{\min}$. The latter scenario corresponds to the one considered in Parish (2016).

SFR16 presented individual B, H, and BH solutions with prescribed values of the controlling parameters and then conducted a sensitivity analysis of the BH solution to the controlling parameter values. A similar analysis is conducted in our study but with the direction of the free-atmosphere geostrophic wind taken as northerly, so $v_{g\infty}$ is always negative. The baseline B, H, and BH solutions were obtained with the default parameter values shown in Table 1 (with $K_d = K_n = 10\,\text{m}^2\,\text{s}^{-1}$ in the H experiment) and were then compared to the corresponding (with the same magnitude of $v_{g\infty}$) southerly solutions from SFR16. After that, the effects of the individual parameter variations on the BH solution were investigated. When the effect of a particular parameter was not being tested, the parameter was set to the default value shown in Table 1.

3. Results

a. Northerly LLJ mechanism

The characteristics of the modeled northerly jets associated with the B, H, and BH mechanisms are shown in Table 2. As one would expect, the B mechanism with a northerly free-atmosphere geostrophic wind results in the same LLJ as the B mechanism with a southerly free-atmosphere geostrophic wind except for the reversed wind direction. This is consistent with the Blackadar (1957) theory, which predicts that geostrophic wind direction should not have an effect on the maximum wind speed of the LLJ. For the H mechanism, the maximum magnitude of the v wind and the height of the v-wind maximum for the northerly LLJ are nearly the same as for the southerly LLJ (both LLJs are weak). The timing of the maximum magnitude of v, however, is substantially different between the two cases. In the northerly jet case, the peak magnitude of v occurs during the daytime (6.3 h after sunrise), unlike the southerly jet case where the peak magnitude of v occurs at night (17.8 h after sunrise). For the BH mechanism, the maximum v magnitude in the northerly jet case is only slightly larger than the free-atmosphere geostrophic wind magnitude and occurs at a height far above of that of typical observed LLJs. The maximum v magnitude is reached at ~1.5 h before sunset. Figure 2 reveals that a weak jet forms at a lower height at night, but its magnitude does not exceed the maximum magnitude of the daytime v. In contrast, for the southerly LLJ case, the maximum magnitude of v is reached ~8.5 h after sunset at an altitude of 480 m, and it is larger than the maximum magnitude v for the cases with the B or H mechanism acting alone.

These preliminary tests indicate that the effects of buoyancy are largely responsible for the difference between the northerly and southerly jet solutions. To shed

TABLE 1. The reference values for the 11 parameters of the analytical solution. The values are the same used in SFR16 except the free-atmosphere geostrophic wind is negative. Times are in hours after sunrise.

Parameter	Value
Coriolis parameter (f)	$8.6 \times 10^{-5}\,\mathrm{s}^{-1}$ ($\varphi = 36.4°\mathrm{N}$)
Free-atmosphere geostrophic wind ($v_{g\infty}$)	$-10\,\mathrm{m\,s}^{-1}$
Slope angle (α)	0.15°
Brunt–Väisälä frequency (N)	$0.01\,\mathrm{s}^{-1}$
Surface buoyancy maximum ($b_{\max}$)	$0.2\,\mathrm{m\,s}^{-2}$
Surface buoyancy minimum ($b_{\min}$)	$-0.2\,\mathrm{m\,s}^{-2}$
Time of buoyancy maximum ($t_{\max}$)	9 h
Time of sunset (t_{set})	12 h
Daytime eddy diffusivity (K_d)	$100\,\mathrm{m}^2\,\mathrm{s}^{-1}$
Nighttime eddy diffusivity (K_n)	$1\,\mathrm{m}^2\,\mathrm{s}^{-1}$
Damping parameter (δ)	$0.2\,\mathrm{day}^{-1}$

light on the role of buoyancy, first consider the case where there is no slope ($\alpha = 0$). In this case, (1) becomes

$$\frac{\partial u}{\partial t} = -fv_{g\infty} + fv + K\frac{\partial^2 u}{\partial z^2}. \tag{10}$$

Since buoyancy is not present in (10), the geostrophic wind in the PBL V_g is equal to the time- and height-invariant free-atmosphere geostrophic wind $v_{g\infty}$, so that

$$V_g = v_{g\infty}. \tag{11}$$

Recall that without a slope or inhomogeneous buoyancy forcing, the nocturnal LLJ forms because of the B mechanism only. In this case, the ageostrophic component of the wind develops during the daytime as a result of the friction force associated with the diffusion of momentum. When eddy diffusivity is reduced at sunset, the ageostrophic wind begins an oscillation around the constant geostrophic wind vector, which leads to the formation of the LLJ.

Now consider the relation between V_g and $v_{g\infty}$ in the presence of an eastward-facing slope with angle α. In this case, (1) becomes

$$\frac{\partial u}{\partial t} = -fv_{g\infty} - b\sin\alpha + fv + K\frac{\partial^2 u}{\partial z^2}. \tag{12}$$

The geostrophic wind V_g in this case is given by the sum of the constant free-atmosphere geostrophic wind and a buoyancy contribution:

$$V_g(z,t) = v_{g\infty} + \frac{1}{f}b\sin\alpha. \tag{13}$$

A similar expression is shown as an approximated function of z^* in appendix A of SFR16. Since buoyancy is time and height dependent, the geostrophic wind must also be time and height dependent. For a northerly jet ($v_{g\infty} < 0$), the geostrophic wind V_g will be at a maximum magnitude when buoyancy is at a minimum and at a minimum when buoyancy is at a maximum. The opposite would be true for a southerly LLJ.

Figure 3 shows the magnitude of the geostrophic wind V_g associated with the BH mechanism as a function of time and height for both the northerly and southerly LLJs. When the evolution of the geostrophic wind in Fig. 3 is compared to the corresponding buoyancy distributions shown in Fig. 4, the association between buoyancy and the geostrophic wind magnitude implied by (13) can be clearly seen. Figures 3 and 4 also help to explain how the eastward-sloping terrain obstructs the development of a northerly nocturnal LLJ. At sunrise ($t = 0$), surface buoyancy is at a minimum, which causes the magnitude of the northerly geostrophic wind to be at a maximum. The comparatively large daytime eddy diffusivity creates a cross-isobaric component of the wind that is directed down the slope toward low pressure. Equation (4) shows that these downslope winds will increase buoyancy through advection of the environmental potential temperature (represented by the $uN^2\sin\alpha$ term). In addition, the daytime heating leads to an increase of surface buoyancy, which is mixed upward by the enhanced eddy diffusivity. This increase in buoyancy creates an upslope-directed force that opposes the downslope component of the wind created by the frictional force. This results in the u-wind component decreasing during the daytime. The buoyancy continues to increase until the time of peak surface buoyancy, and at this time, the magnitude of the northerly geostrophic wind is at its minimum. At sunset,

TABLE 2. The maximum magnitude of the v component of the wind $v_{\max}$, the height of the maximum magnitude v component of the wind $Z_{v_{\max}}$, and time after sunrise of the maximum magnitude v component of the wind $T_{v_{\max}}$ for both a northerly and southerly geostrophic wind for the B, H, and reference BH solutions. The southerly geostrophic wind data are from SFR16.

	Northerly jet			Southerly jet		
Mechanism	$v_{\max}$ ($\mathrm{m\,s}^{-1}$)	$Z_{v_{\max}}$ (m)	$T_{v_{\max}}$ (h)	$v_{\max}$ ($\mathrm{m\,s}^{-1}$)	$Z_{v_{\max}}$ (m)	$T_{v_{\max}}$ (h)
B	−16.8	460	21.0	16.8	460	21.0
H	−11.1	1020	6.3	11.5	1000	17.8
BH	−10.5	3640	10.5	21.1	480	20.5

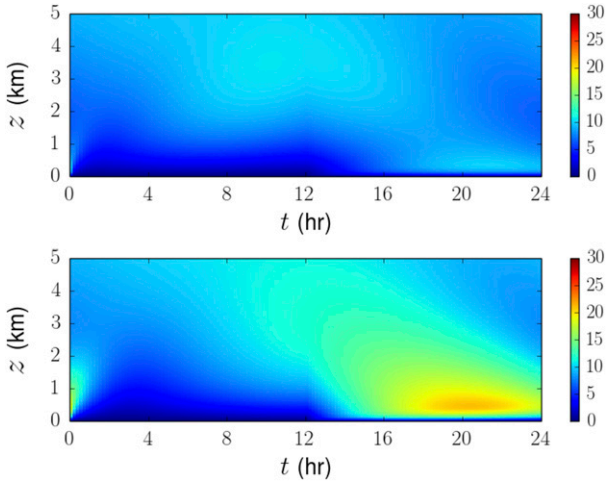

FIG. 2. Wind speed ($m\,s^{-1}$) as a function of time and height corresponding to the reference BH solutions for a $10\,m\,s^{-1}$ magnitude (top) northerly and (bottom) southerly free-atmosphere geostrophic wind. Times are hours after sunrise.

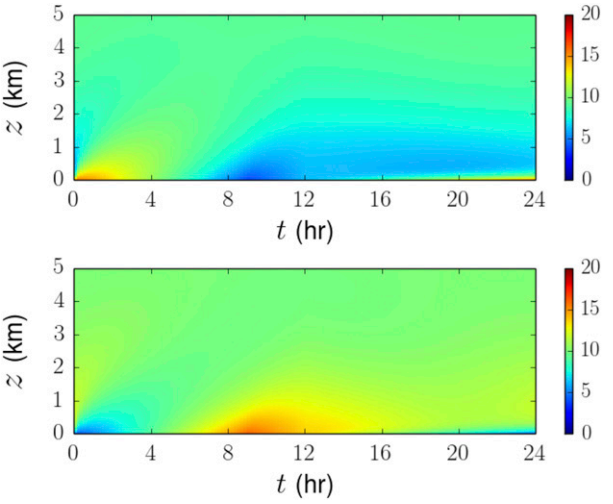

FIG. 3. As in Fig. 2, but for the geostrophic wind magnitude ($m\,s^{-1}$).

when the inertial oscillation begins, the large buoyancy is still present, which limits the magnitude of the northerly geostrophic wind. With the geostrophic wind magnitude being small, the amplitude of the inertial oscillation is also small, which results in a weak LLJ. Figure 4 indicates that large positive buoyancy remains throughout the night for the northerly LLJ (except in the growing stable layer adjacent to the surface). Such retention of positive buoyancy is primarily caused by the flow accelerating down the slope after the onset of the inertial oscillation. The increase in the downslope wind coupled with the ineffective mixing of negative buoyancy by the reduced nighttime eddy diffusivity prevents the northerly geostrophic wind magnitude from increasing substantially at night even though the surface buoyancy is decreasing. This analysis shows that for northerly LLJs over eastward-sloping terrain, the Blackadar and Holton mechanisms are acting out of phase.

b. *Effects of parameter variations*

Because of the detrimental effects of positive buoyancy on the northerly LLJ, stronger northerly LLJs would be expected when buoyancy values are small around the time of the jet initiation. Therefore, setting the values of the controlling parameters of the analytical solution in a manner that decreases buoyancy values during the afternoon should result in stronger northerly LLJs. Results of the calculations with varying parameter values are summarized in Table 3, which contains data for the maximum wind speed beneath 2000 m above ground level (AGL) after sunset. These time and height limitations were imposed on the parameters shown in Table 3 in order to reflect the effect of parameter variations on the nocturnal northerly LLJ, not on the elevated daytime wind maxima. Even though maximum wind speed was used, the contribution from the u-wind component is only $\sim 1\,m\,s^{-1}$.

As expected, changing the maximum daytime surface buoyancy had the greatest effect on the magnitude of the nocturnal northerly LLJ. If the maximum surface buoyancy is increased from its default value, then essentially, no LLJ forms at night as the maximum wind speed ($7.6\,m\,s^{-1}$) remains below the free-atmosphere geostrophic value, but if the surface buoyancy maximum is decreased, a significant LLJ ($17\,m\,s^{-1}$) develops. Reducing the surface buoyancy maximum results in less surface buoyancy available to be mixed upward during the day, thereby reducing buoyancy above the surface. Changing the minimum surface buoyancy at sunrise does not have as great of an effect as changing the daytime surface buoyancy maximum. Nevertheless, decreasing the surface buoyancy minimum does result in slightly stronger nocturnal northerly LLJs.

The role of eddy diffusivity and its temporal variation is more complicated. Daytime and nighttime values of the eddy diffusivity affect the vertical distribution of buoyancy through mixing, and the diffusivity change from the daytime value to the nighttime value triggers the inertial oscillation. Unlike the southerly jet experiments in SFR16, increasing the difference between the daytime and nighttime values of K in the northerly jet case results in only a slightly stronger LLJ ($10.9\,m\,s^{-1}$). The stronger inertial oscillation effect barely overcomes the increased buoyancy because of greater mixing. Reducing the daytime eddy diffusivity prevents an LLJ

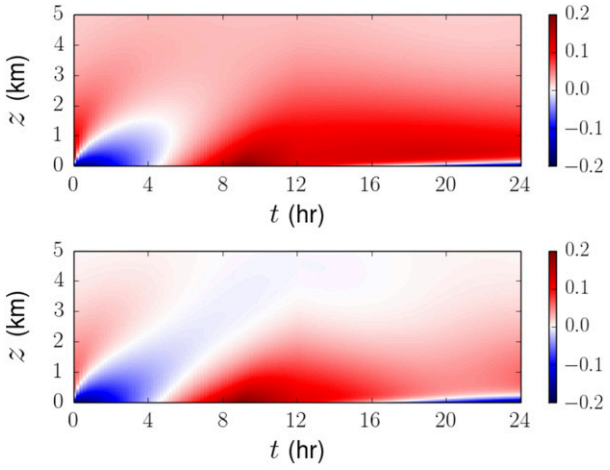

FIG. 4. As in Fig. 2, but for buoyancy ($m\,s^{-2}$).

from developing as the maximum wind speed in this case occurs almost immediately after sunset at a height (1680 m) above that of other LLJs produced by the analytical solution. The reduced buoyancy caused by the smaller daytime eddy diffusivity is not able to compensate for the reduced inertial oscillation effect. Varying the nighttime eddy diffusivity does not substantially change buoyancy values as the mixing is typically small. Increasing the nighttime eddy diffusivity, however, prevents a northerly LLJ from developing (maximum wind speed of 9.3 $m\,s^{-1}$ is below the free-atmosphere geostrophic value) because of the reduced inertial oscillation effect, while decreasing the nighttime eddy diffusivity marginally increases the northerly wind speed maximum (10.9 $m\,s^{-1}$) and causes the maximum to occur at a lower height (180 m).

The free-atmosphere geostrophic wind magnitude significantly impacts the strength of the northerly LLJ. Increasing the northerly geostrophic wind magnitude intensifies the nocturnal northerly LLJ (17.7 $m\,s^{-1}$). This result is unsurprising since a stronger free-atmosphere geostrophic wind represents a stronger background pressure gradient force. Interestingly, the LLJ is more supergeostrophic when there is a stronger free-atmosphere geostrophic wind. When the free-atmosphere geostrophic wind is decreased to 5 $m\,s^{-1}$, the LLJ is actually subgeostrophic.

Another interesting result is related to the effect of the Coriolis parameter on the solution. Increasing the Coriolis parameter (i.e., increasing latitude) results in a slightly stronger northerly LLJ (10.8 $m\,s^{-1}$), while decreasing the Coriolis parameter slightly reduces the magnitude of the wind maximum (9.6 $m\,s^{-1}$). This result is consistent with the climatological studies of Bonner (1968) and Walters et al. (2008), which show that northerly LLJs over the Great Plains occur more frequently at higher latitudes. However, the climatological differences might reflect latitudinal variations in synoptic settings rather than the impact of variations in the Coriolis parameter on inertial oscillations.

TABLE 3. The maximum wind speed V_{max}, height of wind speed maximum $Z_{V_{max}}$, and time of maximum wind speed max $T_{V_{max}}$ for the individual parameter tests for the BH mechanism in northerly LLJs. Winds maxima were limited to those occurring below 2000 m after sunset.

Varied parameter	Experiment	Parameter value	V_{max} ($m\,s^{-1}$)	$Z_{V_{max}}$ (m)	$T_{V_{max}}$ (h)
None	BH	—	10.0	360	21.2
b_{max}	BH b^+_{max}	0.3 $m\,s^{-2}$ ($\Delta b = 0.5\ m\,s^{-2}$)	7.6	1980	13.8
	BH b^-_{max}	0.0 $m\,s^{-2}$ ($\Delta b = 0.2\ m\,s^{-2}$)	17.0	420	20.7
b_{min}	BH b^+_{max}	−0.3 $m\,s^{-2}$ ($\Delta b = 0.5\ m\,s^{-2}$)	10.9	340	21.3
	BH b^-_{max}	0.0 $m\,s^{-2}$ ($\Delta b = 0.2\ m\,s^{-2}$)	8.4	420	21.0
K_d	BH K^+_d	500 $m^2\,s^{-1}$	10.9	400	21.5
	BH K^-_d	20 $m^2\,s^{-1}$	10.4	1680	12.2
K_n	BH K^+_n	5 $m^2\,s^{-1}$	9.3	1980	15.7
	BH K^-_n	0.2 $m^2\,s^{-1}$	10.9	180	21.5
$v_{g\infty}$	BH $v^+_{g\infty}$	15 $m\,s^{-1}$	17.7	400	20.8
	BH $v^-_{g\infty}$	5 $m\,s^{-1}$	4.0	160	24.0
f	BH f^+	$9.7 \times 10^{-5}\ s^{-1}$ ($\varphi = 42°N$)	10.8	360	20.2
	BH f^-	$7.3 \times 10^{-5}\ s^{-1}$ ($\varphi = 30°N$)	9.6	1980	15.7
δ	BH δ^+	1 day^{-1}	11.1	380	21.7
	BH δ^-	0.1 day^{-1}	9.9	360	21.7
t_{max}	BH t^+_{max}	11 h ($t_{set} - t_{max} = 1$ h)	10.2	1980	15.3
	BH t^-_{max}	7 h ($t_{set} - t_{max} = 5$ h)	11.5	360	21.2
t_{set}	BH t^+_{set}	14 h ($t_{set} - t_{max} = 5$ h)	12.1	360	23.2
	BH t^-_{set}	11 h ($t_{set} - t_{max} = 1$ h)	10.7	1980	13.8
N	BH N^+	0.02 s^{-1}	8.1	360	20.2
	BH N^-	0.005 s^{-1}	10.7	360	21.5

As explained in SFR16, the radiative damping parameter δ in (4) ensures periodicity of the 1D LLJ solution (more accurately, its omission precludes the existence of periodic solutions). However, the SFR16 solution was found to be rather insensitive to the actual parameter value. The same is generally true for northerly LLJs, but an increase in the damping parameter does result in slightly stronger northerly LLJs (11.1 m s^{-1}). According to (4), the damping parameter reduces the magnitude of the buoyancy. A larger damping parameter would lead to a greater reduction of buoyancy, which would then promote northerly LLJ development.

The difference between the time of sunset and the time of the surface buoyancy maximum also has an effect on the solution. When this difference was increased by either making the surface buoyancy maximum occur earlier or by delaying the sunset, the northerly LLJ maximum wind speed increased (11.5 and 12.1 m s^{-1}, respectively). A smaller time difference between the two occurrences resulted in slightly weaker (and elevated) wind speed maxima. A larger difference between t_{max} and t_{set} combined with the onset of surface cooling allows the daytime eddy diffusivity to mix out the buoyancy maximum, which lowers buoyancy before sunset and creates a stronger northerly LLJ.

The final parameter tested was environmental Brunt–Väisälä frequency N. Like in SFR16, decreasing N increased the strength of the jet. As seen from (4), N controls the production of buoyancy because of the upslope/downslope advection of the environmental potential temperature $uN^2 \sin\alpha$. Since the daytime x-component wind for a northerly LLJ is downslope (positive u), and at sunset, the initial acceleration is also downslope, a reduced Brunt–Väisälä frequency (weaker ambient stratification) would cause a smaller increase in buoyancy, which results in a smaller decrease in the magnitude of the geostrophic wind and thus provides a stronger LLJ.

An additional test was conducted with a free-atmosphere geostrophic wind of -15 m s^{-1}, surface buoyancy maximum of -0.05 m s^{-2}, surface buoyancy minimum of -0.45 m s^{-2}, Coriolis parameter corresponding to 42°N, and Brunt–Väisälä frequency of 0.008 s^{-1}. The purpose of the test was to model a northerly LLJ where multiple parameter values that were shown to individually favor increases in northerly LLJ wind speeds were acting together. The corresponding solution, illustrated in Fig. 5, predicted an intense nocturnal northerly LLJ with a maximum wind speed of 28.5 m s^{-1}.

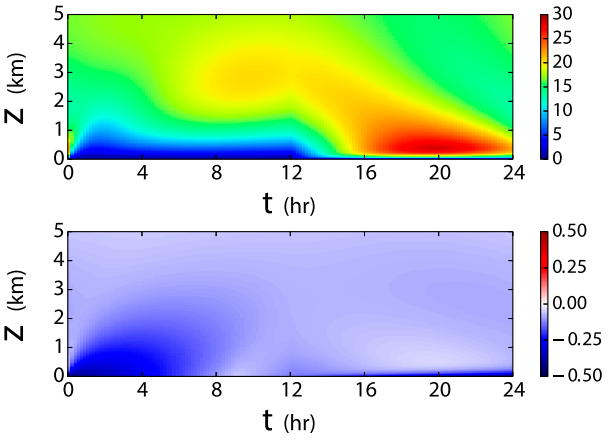

FIG. 5. (top) Wind speed (m s^{-1}) and (bottom) buoyancy (m s^{-2}) as a function of time and height for the BH solution with a northerly geostrophic wind of -15 m s^{-1}, surface buoyancy maximum of -0.05 m s^{-2}, surface buoyancy minimum of -0.45 m s^{-2}, latitude of 42°N, and Brunt–Väisälä frequency of 0.008 s^{-1}. These values all resulted in an increase in northerly LLJ intensity when tested individually.

4. Discussion

Tests of the analytical solution described in the previous section provide insights into the conditions favoring the development of northerly nocturnal LLJs over the Great Plains. The ideal setup for a northerly nocturnal LLJ would include a strong northerly free-atmosphere geostrophic wind over the northern region of the Plains. Daytime buoyancy values in the PBL would be low, and daytime turbulent mixing should be strong. Not surprisingly, a substantial decrease of the eddy diffusivity at sunset is needed to create a strong inertial oscillation. This consideration is consistent with previous theoretical analyses of nocturnal LLJs by Shapiro and Fedorovich (2010) and SFR16.

While at first, the outlined conditions seem reasonable, the manner in which a low-buoyancy requirement can be realized is not obvious. For example, low buoyancy can be achieved by reducing daytime surface heating. Under real conditions, however, surface heating and eddy diffusivity are physically connected. Reducing daytime surface heating would result in less turbulent mixing. If turbulent mixing is reduced, then the inertial effect created by the reduction in turbulence at sunset would be smaller and would limit the strength of the LLJ. This situation could be replicated in the analytical solution by lowering the surface buoyancy maximum and also lowering the daytime eddy diffusivity. This scenario, however, is not favorable for LLJ development, and therefore, reduced daytime surface heating is not likely a key factor in northerly LLJ development.

There is a second scenario that could lead to small buoyancy values over the sloping terrain. Consider a well-mixed tilted PBL over the sloping terrain as

described in Shapiro and Fedorovich (2009). In this well-mixed PBL, the potential temperature is independent of z^*, but the buoyancy varies with height according to

$$b(h^*) = -\frac{g\Delta\theta}{\theta_0} + N^2(h^* + \Delta h^*), \tag{14}$$

where $\Delta\theta$ is the potential temperature change across the capping inversion, θ_0 is a constant reference potential temperature, h^* is an arbitrary distance below the base of the capping inversion in the true vertical direction z^*, and Δh^* is the depth of the capping inversion in the true vertical direction (see Fig. 6). This equation shows that buoyancy depends on the strength of the capping inversion and the free-atmosphere stratification represented by N. If the capping inversion is strong, and the free-atmosphere stratification is weak, then daytime heating can produce a well-mixed PBL associated with a negative near-surface buoyancy. For example, an N of $0.008\,\mathrm{s}^{-1}$ and a capping inversion strength of $\Delta\theta = 4\,\mathrm{K}$ would result in a surface buoyancy value of about $-0.06\,\mathrm{m\,s}^{-2}$. In this case, the PBL would be set up for a strong nocturnal LLJ. Our analytical solution, however, does not directly account for the capping inversion. The effect of a strong capping inversion and weak free-atmosphere stratification would be best represented within our model framework by decreasing both the buoyancy minimum and the buoyancy maximum by the same value. Therefore, it would still be possible to keep the eddy diffusivities at their typical values in a diurnal cycle of strong daytime mixing and reduced mixing at sunset. The buoyancy maximum and minimum values used to create the strong northerly LLJ shown in Fig. 5 are an example of how this effect could be represented in the analytical model.

A strong northerly LLJ (peak winds of $\sim 18\,\mathrm{m\,s}^{-1}$) with similar 1D characteristics as those described in the previous paragraph was observed on 29 September 2016 by the Doppler lidar from the Collaborative Lower Atmospheric Mobile Profiling System 2 (CLAMPS-2) at Norman, Oklahoma (Fig. 7). Before the LLJ developed, the 0000 UTC sounding from Norman, Oklahoma (OUN), showed a well-mixed PBL capped by a 2-km-deep layer of strong static stability (Fig. 8). Above this layer was a region with a more uniform free-atmosphere potential temperature profile. The wind at that time was $\sim 2.6\,\mathrm{m\,s}^{-1}$ from the north-northeast near the surface and increasing in speed to $\sim 15.4\,\mathrm{m\,s}^{-1}$ from the north-northwest at the top of the strong stability layer. The surface buoyancy was $\sim -0.14\,\mathrm{m\,s}^{-2}$. This value was obtained by extrapolating the free-atmosphere potential temperature profile down to the surface and then subtracting the extrapolated free-atmosphere potential temperature from the observed surface potential temperature. Vertical velocities from the CLAMPS-2 Doppler lidar (Fig. 7) and the presence of a well-mixed PBL on the 0000 UTC sounding show that significant mixing was occurring during the day leading up to the northerly LLJ despite the presence of negative surface buoyancy. The combination of negative surface buoyancy and strong mixing near the time of sunset facilitated the development of the northerly LLJ on this night.

Thus far, our discussion of northerly LLJs does not indicate that diurnal PBL processes alone can result in the maximum in occurrence of northerly LLJs over the Great Plains. Since diurnal heating of eastward-sloped terrain is inimical to the development of northerly nocturnal LLJs, one might think that nocturnal northerly LLJs should be at a minimum frequency over the region. The above example does suggest, however, that the sloping terrain is likely contributing to the development of northerly LLJ and may affect their frequency over the Great Plains.

Using the results from the analytical model as a guide, we propose the following theory for the cause of the northerly LLJ maximum. As previously mentioned, a strong capping inversion leads to lower buoyancy values over the slope. Because of the dependence of the geostrophic wind on buoyancy, northerly low-level geostrophic winds over the slope would be enhanced when outbreaks of cold air with strong inversions occur over the sloping terrain. The stronger northerly geostrophic winds would tend to increase the actual low-level winds, which would create jetlike wind profiles. Under the assumption that buoyancy is horizontally uniform along the surface, this same type of cold-air outbreak over flat terrain would not result in the same jet profile, as buoyancy would not factor into the geostrophic wind. Because of the enhancement of the northerly geostrophic wind during cold-air outbreaks over the Great Plains, the spatial climatologies would detect more northerly LLJs over the region. Bonner (1968, p. 837) mentioned that northerly LLJs were often associated with ''shallow cold highs'' with ''weak southerly flow aloft.'' This observation would support the idea that the climatological frequency maximum over the Great Plains is due to the enhancement of the low-level northerly geostrophic wind during cold-air outbreaks. This mechanism would also explain the association between northerly LLJs and cold fronts south of the LLJ locations (Bonner 1968; Whiteman et al. 1997). The environment behind cold fronts would typically be associated with negative buoyancy over the slope, and this negative buoyancy would enhance the postfrontal LLJs described by Ostdiek and Blumen (1997). Obviously, since cold-frontal passages and associated cold-air

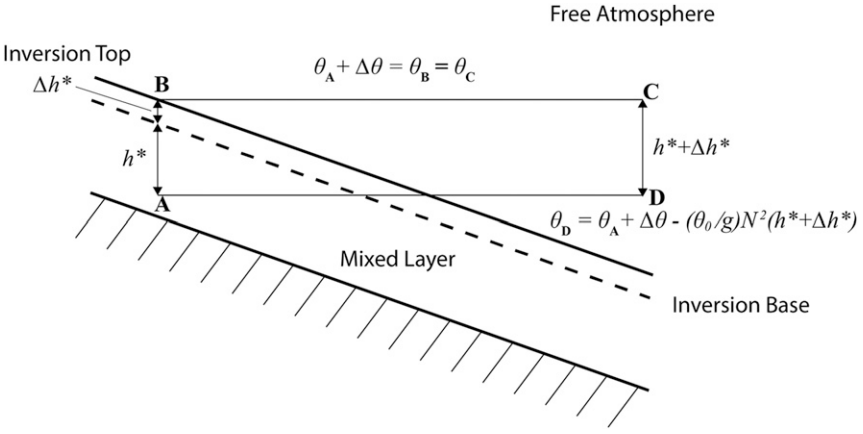

FIG. 6. A schematic cross section of a well-mixed tilted PBL over a slope [adapted from Shapiro and Fedorovich (2009)]. The dashed line is the bottom of the capping inversion while the diagonal line passing through B is the top of the capping inversion. Point A is any location in the mixed layer, point B is directly above point A in the true vertical direction at the capping inversion top, point C is in the free atmosphere at the same elevation as B, and point D is in the free atmosphere at the same elevation as A and directly below C. Line BC is an environmental isentrope. Buoyancy at point A is $b(h^*) = (g/\theta_0)(\theta_A - \theta_D)$.

outbreaks do not depend on the diurnal cycle, there would be no clear preferred time of occurrence for these LLJs. The Bonner (1968) and Walters et al. (2008) climatologies did show an early morning maximum in occurrence, however. This is due to the northerly nocturnal LLJs that are primarily driven by the inertial oscillation mechanism. Even though our study suggests that northerly nocturnal LLJs resulting from diurnal boundary layer processes should be at a minimum over the Great Plains because of the negative effect of the

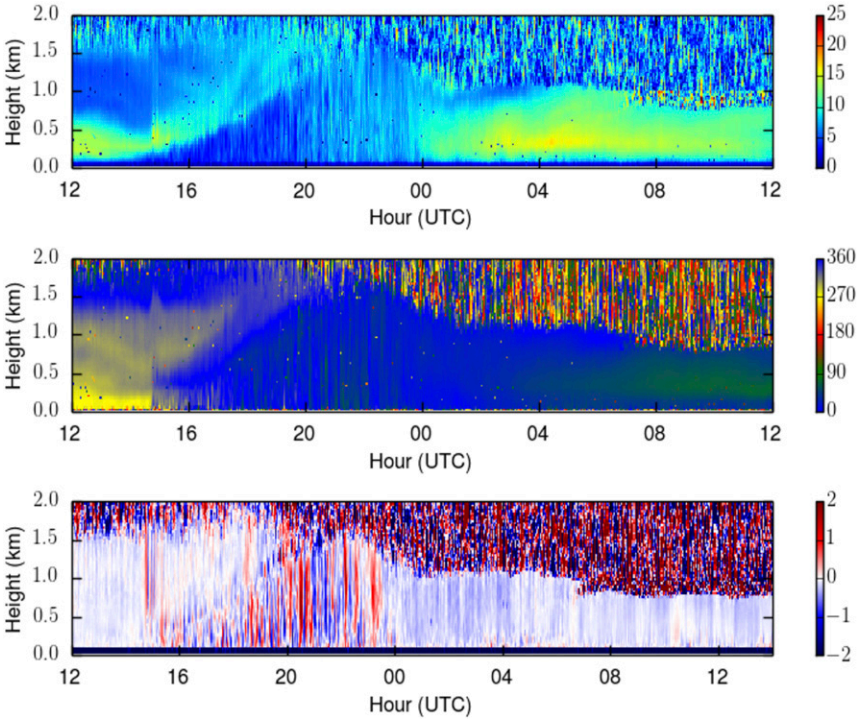

FIG. 7. Observations from the CLAMPS-2 Doppler lidar from 1200 UTC 28 Sep to 1200 UTC 29 Sep 2016. The (top) wind speed ($m\,s^{-1}$), (middle) wind direction (degrees), and (bottom) vertical velocities ($m\,s^{-1}$) were obtained with a 60° velocity–azimuth display (VAD) scanning technique.

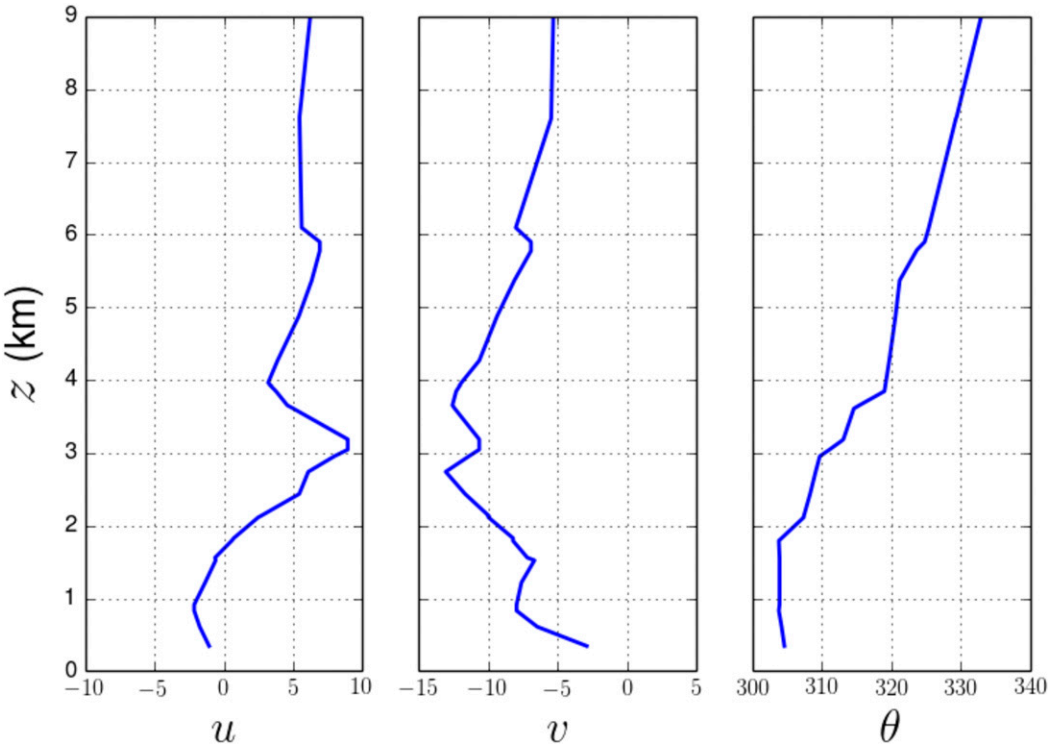

FIG. 8. Profiles of (left) u (m s^{-1}), (center) v (m s^{-1}), and (right) potential temperature (K) from the 0000 UTC 29 Sep 2016 sounding at OUN.

Holton mechanism, they still do occur (see Fig. 7) and would cause twice-daily sounding climatologies to show an early morning maximum in northerly LLJ occurrence.

The analysis in this study is limited by the 1D nature of our model, as along-slope variations in buoyancy are ignored. However, 2D effects likely do play a role in northerly LLJ development through enhancing or opposing 1D effects. Therefore, the mechanisms described in this paper may not explain all northerly LLJ occurrences. For example, a thermal wind resulting from horizontal synoptic-scale temperature gradients (not to be confused with thermal wind resulting from uniform buoyancy over the slope) is not included in our analytical consideration. Depending on the direction of the temperature gradient, the geostrophic wind in the PBL can either be enhanced or reduced and could lead to an LLJ-like wind profile. More work is required to understand how horizontal heterogeneity affects the northerly LLJ.

5. Conclusions

Previous studies of the Great Plains LLJs identified a maximum frequency in northerly LLJs over the northern Great Plains, but no studies have examined the forcing behind this phenomenon. Application of the analytical model developed by SFR16 to the PBL flow driven by a northerly free-atmosphere geostrophic wind revealed that nocturnal northerly LLJs are stronger when buoyancy values in the boundary layer are small at sunset. Changing values of almost all controlling parameters of the solution (except for the eddy diffusivity) in a manner that would decrease buoyancy at sunset resulted in a stronger northerly nocturnal LLJ. A large decrease of eddy diffusivity from day to night was required for the development of a significant northerly nocturnal LLJ. Such a decrease was found to produce a strong inertial effect that was able to partially overcome the negative effect of positive buoyancy. The process of diurnal heating/cooling variation alone, however, cannot explain the northerly LLJ maximum over the Great Plains. In fact, nocturnal northerly LLJs resulting from diurnal PBL processes alone should occur less frequently over the Great Plains since the diurnal change in buoyancy over the slope (Holton mechanism) is unfavorable for these LLJs.

The northerly LLJ climatological maximum is likely the result of the enhancement of the lower-atmospheric northerly geostrophic wind by negative buoyancy over the eastward-sloping terrain. When a strong capping inversion and weak free-atmosphere stratification are present, negative buoyancy values may occur in the PBL

above the slope. Since the geostrophic wind over the sloping terrain is dependent on buoyancy, the northerly geostrophic wind magnitude would be increased by this negative buoyancy. The enhancement of the northerly geostrophic wind can result in LLJ-like profiles, which would be detected in the LLJ climatologies. Such conditions would tend to occur after frontal passages and would enhance postfrontal LLJs. Northerly LLJs that are created by this mechanism explain the weaker diurnal dependence of these LLJs found in climatologies and the association between the LLJs and cold-frontal passages. Future research should attempt to seek more observational evidence about northerly LLJs and improve the understanding of the 2D effects in the LLJ formation.

Acknowledgments. We thank Dave Turner for providing the observational data from CLAMPS-2. This research was supported by the National Science Foundation under Grant AGS-1359698.

REFERENCES

Banta, R. M., and Coauthors, 1998: Daytime buildup and nighttime transport of urban ozone in the boundary layer during a stagnation episode. *J. Geophys. Res.*, **103**, 22 519–22 544, doi:10.1029/98JD01020.

——, R. K. Newsom, J. K. Lundquist, Y. L. Pichogina, R. L. Coulter, and L. Mahrt, 2002: Nocturnal low-level jet characteristics over Kansas during CASES-99. *Bound.-Layer Meteor.*, **105**, 221–252, doi:10.1023/A:1019992330866.

——, Y. L. Pichugina, N. D. Kelley, R. M. Hardesty, and W. A. Brewer, 2013: Wind energy meteorology: Insight into wind properties in the turbine-rotor layer of the atmosphere from high-resolution Doppler lidar. *Bull. Amer. Meteor. Soc.*, **94**, 883–902, doi:10.1175/BAMS-D-11-00057.1.

Bao, J. W., S. A. Michelson, P. O. G. Persson, I. V. Djalalova, and J. M. Wilczak, 2008: Observed and WRF-simulated low-level winds in a high-ozone episode during the Central California Ozone Study. *J. Appl. Meteor. Climatol.*, **47**, 2372–2394, doi:10.1175/2008JAMC1822.1.

Blackadar, A. K., 1957: Boundary layer wind maxima and their significance for the growth of nocturnal inversions. *Bull. Amer. Meteor. Soc.*, **38**, 283–290.

Bonner, W. D., 1968: Climatology of the low level jet. *Mon. Wea. Rev.*, **96**, 833–850, doi:10.1175/1520-0493(1968)096<0833:COTLLJ>2.0.CO;2.

——, and J. Paegle, 1970: Diurnal variations in boundary layer winds over the south-central United States in summer. *Mon. Wea. Rev.*, **98**, 735–744, doi:10.1175/1520-0493(1970)098<0735:DVIBLW>2.3.CO;2.

Cosack, N., S. Emeis, and M. Kuhn, 2007: On the influence of low-level jets on energy production and loading of wind turbines. *Wind Energy: Proceedings of the Euromech Colloquium*, J. Peinke, P. Schaumann, and S. Barth, Eds., Springer, 325–328, doi:10.1007/978-3-540-33866-6_61.

Darby, L. S., K. J. Allwine, and R. M. Banta, 2006: Nocturnal low-level jet in a mountain basin complex. Part II: Transport and diffusion of tracer under stable conditions. *J. Appl. Meteor. Climatol.*, **45**, 740–753, doi:10.1175/JAM2367.1.

French, A. J., and M. D. Parker, 2010: The response of simulated nocturnal convective systems to developing low-level jets. *J. Atmos. Sci.*, **67**, 3384–3408, doi:10.1175/2010JAS3329.1.

Holton, J. R., 1967: The diurnal boundary layer wind oscillation above sloping terrain. *Tellus*, **19**, 199–205, doi:10.1111/j.2153-3490.1967.tb01473.x.

Klein, P. M., X. M. Hu, and M. Xue, 2014: Impacts of mixing processes in nocturnal atmospheric boundary layer on urban ozone concentrations. *Bound.-Layer Meteor.*, **143**, 159–175, doi:10.1007/s10546-013-9864-4.

Maddox, R. A., 1983: Large-scale meteorological conditions associated with midlatitude, mesoscale convective complexes. *Mon. Wea. Rev.*, **111**, 1475–1493, doi:10.1175/1520-0493(1983)111<1475:LSMCAW>2.0.CO;2.

Means, L. L., 1954: A study of the mean southerly wind maximum in low levels associated with a period of summer precipitation in the Middle West. *Bull. Amer. Meteor. Soc.*, **35**, 166–170.

Ostdiek, V., and W. Blumen, 1997: A dynamic trio: Inertial oscillation, deformation frontogenesis, and the Ekman–Taylor boundary layer. *J. Atmos. Sci.*, **54**, 1490–1502, doi:10.1175/1520-0469(1997)054<1490:ADTIOD>2.0.CO;2.

Parish, T. R., 2000: Forcing of the summertime low-level jet along the California coast. *J. Appl. Meteor.*, **39**, 2421–2433, doi:10.1175/1520-0450(2000)039<2421:FOTSLL>2.0.CO;2.

——, 2016: A comparative study of the 3 June 2015 Great Plains low-level jet. *Mon. Wea. Rev.*, **144**, 2963–2979, doi:10.1175/MWR-D-16-0071.1.

Pitchford, K. L., and J. London, 1962: The low-level jet as related to nocturnal thunderstorms over the Midwest United States. *J. Appl. Meteor.*, **1**, 43–47, doi:10.1175/1520-0450(1962)001<0043:TLLJAR>2.0.CO;2.

Ranjha, R., M. Tjernström, A. Semedo, G. Svensson, and R. M. Cordoso, 2015: Structure and variability of the Oman coastal low-level jet. *Tellus*, **67A**, 25285, doi:10.3402/tellusa.v67.25285.

Shapiro, A., and E. Fedorovich, 2009: Nocturnal low-level jets over a shallow slope. *Acta Geophys.*, **57**, 950–980.

——, and ——, 2010: Analytical description of a nocturnal low-level jet. *Quart. J. Roy. Meteor. Soc.*, **136**, 1255–1262, doi:10.1002/qj.628.

——, ——, and S. Rahimi, 2016: A unified theory for the Great Plains nocturnal low-level jet. *J. Atmos. Sci.*, **73**, 3037–3057, doi:10.1175/JAS-D-15-0307.1.

Song, J., K. Liao, R. L. Coulter, and B. M. Lesht, 2005: Climatology of the low-level jet at the Southern Great Plains Atmospheric Boundary Layer Experiments site. *J. Appl. Meteor.*, **44**, 1593–1606, doi:10.1175/JAM2294.1.

Stensrud, D., 1996: Importance of low-level jets to climate: A review. *J. Climate*, **9**, 1698–1711, doi:10.1175/1520-0442(1996)009<1698:IOLLJT>2.0.CO;2.

Storm, B., J. Dudhia, S. Basu, A. Swift, and I. Giammanco, 2009: Evaluation of Weather Research and Forecasting Model on forecasting low-level jets: Implications for wind energy. *Wind Energy*, **12**, 81–90, doi:10.1002/we.288.

Trier, S. B., and D. B. Parsons, 1993: Evolution of environmental conditions preceding the development of a nocturnal mesoscale convective complex. *Mon. Wea. Rev.*, **121**, 1078–1098, doi:10.1175/1520-0493(1993)121<1078:EOECPT>2.0.CO;2.

Uccellini, L. W., 1980: On the role of upper tropospheric jet streaks and leeside cyclogenesis in the development of low-level jets in the Great Plains. *Mon. Wea. Rev.*, **108**, 1689–1696, doi:10.1175/1520-0493(1980)108<1689:OTROUT>2.0.CO;2.

——, and D. R. Johnson, 1979: The coupling of upper and lower tropospheric jet streaks and implications for the development of severe convective storms. *Mon. Wea. Rev.*, **107**, 682–703, doi:10.1175/1520-0493(1979)107<0682:TCOUAL>2.0.CO;2.

Vera, C., and Coauthors, 2006: The South American Low-Level Jet Experiment. *Bull. Amer. Meteor. Soc.*, **87**, 63–77, doi:10.1175/BAMS-87-1-63.

Walters, C. K., J. A. Winkler, R. P. Shadbolt, J. van Ravensway, and G. D. Bierly, 2008: A long-term climatology of southerly and northerly low-level jets for the central United States. *Ann. Assoc. Amer. Geogr.*, **98**, 521–552, doi:10.1080/00045600802046387.

Whiteman, C. D., X. Bian, and S. Zhong, 1997: Low-level jet climatology from enhanced rawinsonde observations at a site in the Southern Great Plains. *J. Appl. Meteor.*, **36**, 1363–1376, doi:10.1175/1520-0450(1997)036<1363:LLJCFE>2.0.CO;2.

Zhong, S., J. D. Fast, and X. Bian, 1996: A case study of the Great Plains low-level jet using wind profiler network data and a high-resolution mesoscale model. *Mon. Wea. Rev.*, **124**, 785–806, doi:10.1175/1520-0493(1996)124<0785:ACSOTG>2.0.CO;2.

Zunckel, M., G. Held, R. A. Preston-Whyte, and A. Joubert, 1996: Low-level wind maxima and the transport of pyrogenic products over southern Africa. *J. Geophys. Res.*, **101**, 23 745–23 755, doi:10.1029/95JD02602.